Preprints (www.preprints.org) | NOT PEER-REVIEWED | Posted: 19 August 2022 doi:10.20944/preprints202208.0360.v1

Communication

Two Decades-long Satellite Observations of Carbon Monoxide Confirm the Northern Hemispheric Wildfires Increase

Leonid Yurganov[1*] and Vadim Rakitin [2]

[1] University of Maryland Baltimore County, Baltimore, MD, 21250, USA (retired)
[2] A.M. Obukhov Institute of Atmospheric Physics, RAS, Moscow, Russia
* Correspondence: leonid.yurganov@gmail.com;

Abstract: Biomass burning is an important and changing component of the global and hemispheric carbon cycles. Boreal forest fires in Russia and Canada are significant sources of greenhouse gases carbon dioxide (CO_2) and methane (CH_4). The influence of carbon monoxide (CO) on the greenhouse effect is practically absent: its main absorption bands of 4.6 and 2.3 μm are far away from the climatically important spectral regions. Meanwhile, CO concentrations in fire plumes are closely related to CO_2 and CH_4 emissions from fires. On the other hand, satellite measurements of CO are much simpler than those for the aforementioned gases. The Atmospheric Infrared Sounder (AIRS) provides a satellite-based CO data set since October, 2002 up to now. This communication presents estimates of CO emissions from biomass burning north of 30° N using a simple two-box mass-balance model. These results correlate closely with independently estimated CO emissions from the GFED4 bottom-up data base. Both ones reported record high emissions in 2021 throughout two decades, double the annual emissions comparing to the previous years. There have been two years with extremely high emissions (2003 and 2021), but for the rest of data upward trend with a rate of 3.6 ± 2.2 Tg CO yr^{-2} (4.8 ± 2.7% yr^{-1}), was found. A similar rate of CO emission follows from the GFED4 data.

Keywords: Thermal Infrared satellite data; carbon monoxide; boreal fires; carbon dioxide

1. Introduction

Boreal forest fires (wildfires) in the Northern hemisphere have various impacts on the environment and on the climate system. Changes in evapotranspiration, surface heat regime, productivity and soil respiration, postfire changes of albedo on the burned areas and many other effects are just some examples of adverse climatic effects [1]. Emissions of greenhouse gases are in the row of these phenomena. Estimating the amount of greenhouse gases emitted by natural fires is not simple. A so called "bottom-up" approach is based on burned areas and assimilates data on dry organic matter per unit of burned area, emission factors for specific gases, and types of burning and/or smoldering [2]. Many parameters in these calculations are not known accurately. Especially, Siberian fires are most difficult objects due to extremely rare ground network of observations. Nevertheless, a significant progress has been achieved in this technique by now [3, 4].

In another approach, called "top-down" or "inversion", GHG emissions are derived from measurements of gas concentrations in the atmosphere using various sensors, ground-based, aeronautical or satellite. The advantage of satellite concentration measurements over others is their global coverage. The main disadvantage of satellite Thermal IR (TIR) methods is their low accuracy for the planetary boundary layer that is primarily polluted by fires. Therefore, they need to be corrected for lower sensitivity compared to more accurate ground-based spectroscopic solar tracking measurements. Validation is necessary, but in any case, the current validation network is not dense enough. However, the combination of these two independent approaches to the study of greenhouse gas emissions seems promising.

© 2022 by the author(s). Distributed under a Creative Commons CC BY license.

Preprints (www.preprints.org) | NOT PEER-REVIEWED | Posted: 19 August 2022 doi:10.20944/preprints202208.0360.v1

Carbon monoxide (CO) is a second product of wildfires after carbon dioxide (CO_2). Its background concentration is ~4000 less than that for CO_2. The strong CO fundamental absorption band near 4.6 μm wavelength is just slightly overlapped by H_2O lines. Therefore, this species has been a widely recognized proxy for wildfires and urban emissions [5, 6]. The two longest satellite CO data sets are presently available. The Measurement Of Pollution in The Troposphere (MOPITT, 2000 - now) [7] and Atmospheric Infrared Sounder (AIRS, 2002 - now) [8] provide total columns (TC) and profiles globally. Annual concentrations of carbon monoxide have been decreasing since 2000 [7].. The decline is particularly noticeable in the Northern Hemisphere. This is caused by technological and regulatory innovations in transport and industry [7]. Summer year-to-year CO fluctuation were caused by biomass burning [6, 9, 10].

First attempt to estimate CO emissions from fires in 2002-2003. based on satellite data in combination with ground-based sampling in the High Northern Hemisphere (HNH, 30° N - 90° N) was undertaken based on the mass balance model [9]. Previously, this model was developed to study the boreal fires of 1998 [10]. An alternative to the box model is the global three-dimensional transport model. Such a model was applied to the MOPITT dataset for 2000-2017 [11] and inferred surface fluxes of CO from many sources, with a spatial resolution of 3.75° longitude × 1.9° latitude. Global wildfires 2000-2019 were specially considered in [12].

In this report, we estimated all CO emissions from HNH fires from 2002 to 2021 using the box model described in previous publications [9, 10] with the same parameters (characterizing, for example, photochemical removal, air exchange between the tropical and extratropical northern hemisphere, etc.).). Comparison with independent estimates of GFED4 [3] showed reasonable random differences between the two monthly datasets of less than ±10 Tg CO mon-1 for most of the data except for a few points. Both the bottom-up GFED4 method and the top-down AIRS method clearly show an upward trend in forest fire emissions over the past 20 years.

2. Materials and Methods

2.1. AIRS data and validation

AIRS is a diffraction grating spectrometer that was launched in a sun-synchronous polar orbit in May 2002 on board the Aqua satellite [8]. The instrument scans ± 48.3° from the nadir, which provides almost full global daily coverage. Spectral resolution is 1.79 cm^{-1} at the CO fundamental absorption band near 4.6 μm wavelength. The instrument has 13.5 km spatial resolution at nadir. Currently (August, 2022), the AIRS is still operational. A new version 7 of the data [13] is characterized by: improved consistency between day and night water vapor, improved temperature products, improved AIRS IR only retrievals, especially in the high latitude regions, removal of ambiguity in surface classification in the infrared-only (IR-only) retrieval algorithm. Monthly and daily average Level 3 between October, 2002 and May, 2022, for ascending and descending orbits are available on-line on a 1°x1° latitude/longitude grid: https://disc.gsfc.nasa.gov/datasets/, AIRS3STM_7.0 (monthly) and AIRS3STD_7.0. (daily). A reduced sensitivity of AIRS CO to lower troposphere required a correction coefficient (see section 3.1).

The chosen box model deals with monthly total amounts of gas in the box. For our needs we average the total column CO for ascending orbits in molec cm^{-2} (or the vertically averaged volume mixing ratio Xco in ppb) over HNH. After that it is multiplied by the area of the box to get the total amount of CO. Xco for validation are regularly retrieved from spectrally resolved IR radiation recorded by Bruker IFS 125HR sun-tracking Fourier Transform interferometers of ~0.02 cm^{-1} resolution at the Total Carbon Column Observing Network (TCCON) [14]. The Zvenigorod Scientific Station of the Obukhov Institute of Atmospheric Physics is equipped with a diffraction grating sun-tracking spectrometer with a spectral resolution about 0.2 cm^{-1} [15]. The AIRS L3 daily means for the grid cells coinciding with nine locations of validation sites (Table 1) were compared with Xco determined from the ground.

Preprints (www.preprints.org) | NOT PEER-REVIEWED | Posted: 19 August 2022 doi:10.20944/preprints202208.0360.v1

2.2. Mass-balance box model

A box model approach is an alternative to a global Chemical Transport Model (CTM). It is based on a general idea of a relatively slow exchange of air between the HNH and the Low Northern hemisphere (LNH, 0° - 30º N). Wildfires emit CO and this excess CO is quickly spread over the HNH. Leaks to the LNH (transport loss) were estimated from an available CTM model [10, 16]. A significant part of the pyrogenic CO is oxidized by tropospheric hydroxyl OH (Eq 4) and is counted as well.

A calculation procedure was as follows.

1. Satellite-measured CO volume mixing ratio (VMR) profiles are supplied for 24 standard air layers from surface to pressure 1.0 hPa with different pressure thicknesses Δp(i) in hPa, where i is from 1 to 24. VMR averages weighted by Δp(i) were calculated for the sake of comparability with validation network TCCON. Conversion of Xco (ppb) into TC (molec cm^{-2}) were performed as follows: $TC = Xco\ 2.12 \cdot 10^{13} \cdot \Sigma(\Delta p(i))$.

2. The average seasonal cycle over 48 months (4 years) since January 2004 was calculated and assumed as a fire-free standard cycle.

3. The CO trend that is assumed not to be connected with fire variations was calculated for cold February-March months of all years using the fifth order polynomial approximation and applied to all data.

5. The HNH box-averaged CO TC was subtracted by the trend and the seasonal cycle (see Appendix) to represent the TC perturbed by fires. Then it was multiplied by the area of the HNH to get monthly fire-induced total mass anomaly M'_{HNH} in Tg.

6. The anomaly was divided by 0.73 to correct for a reduced sensitivity of measured CO to changes in real CO (see validation section below).

7. Loss terms in the Eqs. 2 and 3 were calculated (see Appendix).

8. The wildfire emission P' was calculated as a sum of monthly changes of M'_{HNH} and two loss terms, transport into the LNH, L_{trans}, and loss of CO due to a reaction with hydroxyl (OH), L_{chem}; quote marks mean deviations from the 2004-2007 background (Eq. 1).

$$P' = \Delta M'_{HNH}/\Delta t + L_{trans} + L_{chem}, \quad (1)$$

$$L_{trans} = (M_{HNH} - M_{LNH})/\tau_{trans}, \quad (2)$$

$$L_{chem} = M'_{HNH}/\tau_{chem}, \quad (3)$$

$$CO + OH = CO_2 + H, \quad (4)$$

$$\tau_{chem} = 1/[OH] \cdot k, \quad (5)$$

$$k = 1.5*10^{-13} (1+0.6 \cdot p)\ cm^3\ molec^{-1}\ s^{-1}, \quad (6)$$

where τ_{trans} was calculated using a 3-D GEOS-CHEM global CTM [10, 16] . [OH] is hydroxyl concentration [17] averaged over HNH, k is the reaction (4) rate constant [18], p is air pressure in hPa. τ_{chem} varied between 1.4 and 27 months in July and in December, respectively [10]. τ_{trans} and τ_{chem} are tabulated in Appendix.

2.3. Validation results

The ground-based TCCON CO measurements for summer months July-August 2013-2021 were used for validation. Figure 1 summarizes comparisons between daily mean Xco measured by ground-based facilities ("ground truth") and the AIRS. Parameters of the least squares linear regression are listed in Table 1. All stations are located to the north of 30° N. Averaged slope of regression lines is 0.73 ppb/ppb with standard deviation 0.14 ppb/ppb. A 19%-scatter in slopes is explained by different conditions in the validation

Preprints (www.preprints.org) | NOT PEER-REVIEWED | Posted: 19 August 2022 doi:10.20944/preprints202208.0360.v1

sites, e.g., a proximity to fires. For example, the location of Tsukuba, Japan, that is close to Tokyo, is more influenced by urban pollution, than by biomass burning. A lower-temperature source leads to a lower altitude of polluted layers and lower slope. Physical meaning of the slope is the empirical sensitivity: a response of AIRS-derived Xco to a unity change of the true value. The slope, averaged over all nine sites, was used for correction of AIRS-detected CO variations. Interceptions (Table 1) are irrelevant to sensitivity; emission rate is proportional to the monthly change in Xco, not to concentration itself. The biases in absolute values are caused by different conditions in sites and method specifics; they are also irrelevant to the anomaly analysis.

3. Results

3.1. Xco measured by AIRS

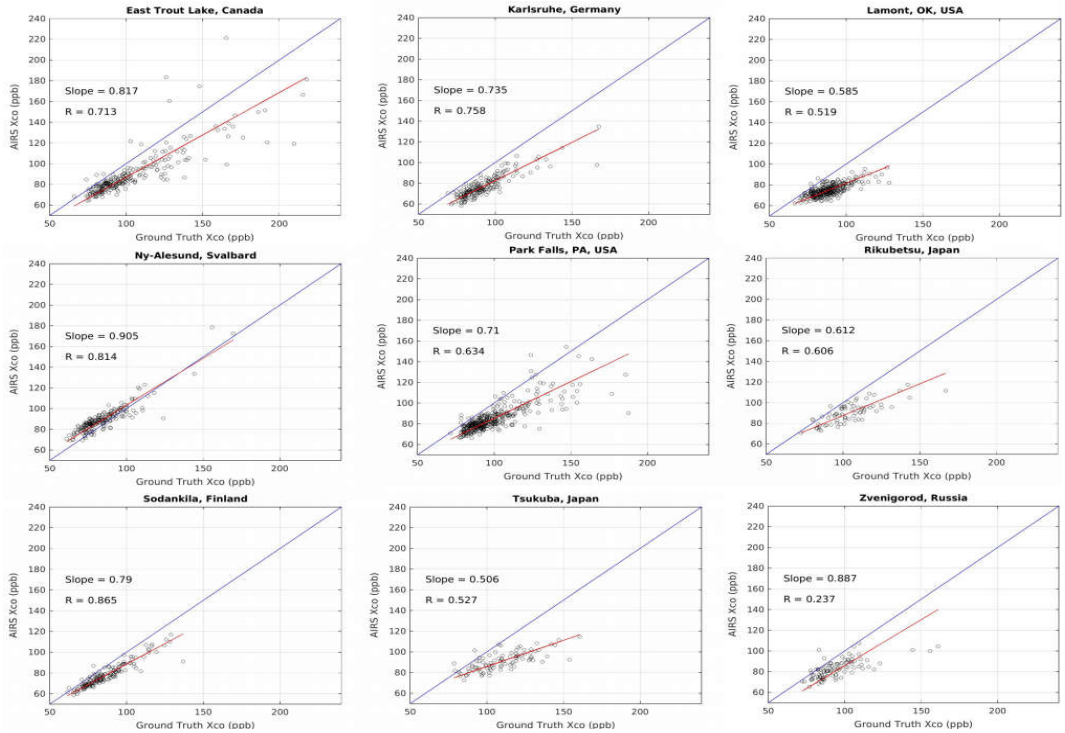

Figure 1. Daily mean Xco measured by AIRS compared with ground-based network.

Table 1. Validation sites. Locations and parameters of linear regression.

Site	Latit.; Longit.	Slope	Interseption	R
E. Trout Lake, Canada	54.35 ; -104.99	0.82	5.43	0.71
Karlsruhe, Germany	49.1; 8.438	0.74	9.23	0.76
Lamont, OK, USA	36.604; -97.486	0.58	23.25	0.52
Ny-Alesund, Svalbard	78.9 ; 11.9	0.90	13.01	0.81
Park Falls, PA, USA	45.945; -90.273	0.71	14.41	0.63
Rikubetsu, Japan	43.4567; 143.7661	0.61	26.37	0.61
Sodankyla, Finland	67.3668; 26.631	0.79	9.67	0.86
Tsukuba, Japan	36.0513 ; 140.1215	0.51	35.38	0.53
Zvenigorod, Russia	55.6957; 36.4454	0.89	-2.64	0.24

Figure 2 presents original AIRS measurements and trends. CO concentrations are impacted by emissions from incomplete combustion in transport and industry. The improvements in technology that reduce anthropogenic emissions leads to a long-term downward trend [11]. Seasonal variations for years with small wildfires have a maximum

Preprints (www.preprints.org) | NOT PEER-REVIEWED | Posted: 19 August 2022 doi:10.20944/preprints202208.0360.v1

in March and a minimum in August [19]. They are determined mainly by OH concentrations, which are minimal in dark and cold seasons. The maximum effect of biomass burning is observed in summer. Both inter-annual variations and increasing trend of summer CO peaks are evident even in the original record. The period of minimal summer disturbances (2004-2007) was taken for calculate the standard seasonal cycle. The original data have been modified in attempt to eliminate the trend and seasonal changes. The trend was defined as a fifth degree polynomial for February-March 2004-2007 data and applied to all results. Therefore, the oscillating thin black line represents a "background". In other words, this line is taken as Xco for no (or negligible) biomass burning emissions for all years. A difference ("CO anomaly") between the red line (measured Xco) and the thin black line (background) is displayed as green dots. This anomaly is considered as a net effect of biomass burning. Verification efforts revealed an underestimation by about 30% of measured anomaly; this has been corrected accordingly. In what follows it was used as input for the box model. Small negative anomalies leading to negative emissions (Figure 3), reflect inaccuracies associated with assumed assumptions and/or other irregularities in CO emissions (e.g., the 2008-2009 economic downturn or the impact of 2020-2021 COVID-19). Most striking is the record CO spike in July-August 2021. Also note the rapid increase in CO anomalies between June and August of each year and subsequent gradual decrease due to photochemical and transport extinction with time scales of several months.

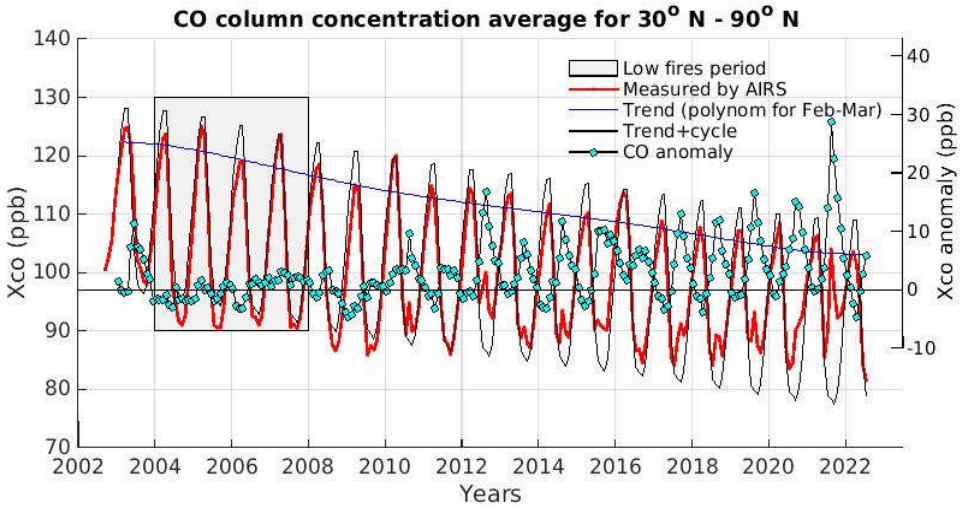

Figure 2. Original data, trend, seasonal cycle + trend (left scale), and fire-induced CO anomaly (right scale). Units are vertically averaged VMR in ppb.

3.2. Fire emissions

Monthly HNH CO emissions from fires calculated using our box model are presented in Figure 3 as a function of time. As a rule, maximum emissions occurred in July, sometimes in August. Months of maximum concentration (e.g. August 2021) usually followed months of maximum emission (July 2021). The GFED4 CO data are consistent with the AIRS data. The scatter plot (Fig. 4) shows a strong correlation between the monthly emissions obtained by these two independent methods (slope 0.84 ± 0.07, 95% confidence interval, correlation coefficient R = 0.69). The absolute values of emissions differ by less than ~10 Tg/month in most data, only three circled summer points are scattered. In all three cases, the AIRS data were lower than the emissions estimated by

Preprints (www.preprints.org) | NOT PEER-REVIEWED | Posted: 19 August 2022 doi:10.20944/preprints202208.0360.v1

GFED4. During these months (July and August) the most severe fires occur. It is reasonable to assume that the additional CO is in the lower troposphere, and the decrease in the sensitivity of the TIR instruments leads to an underestimation. In order to confirm remotely sensed data with more representativeness, ground control points are needed closer to the fire areas than the TCCON sites (see above).

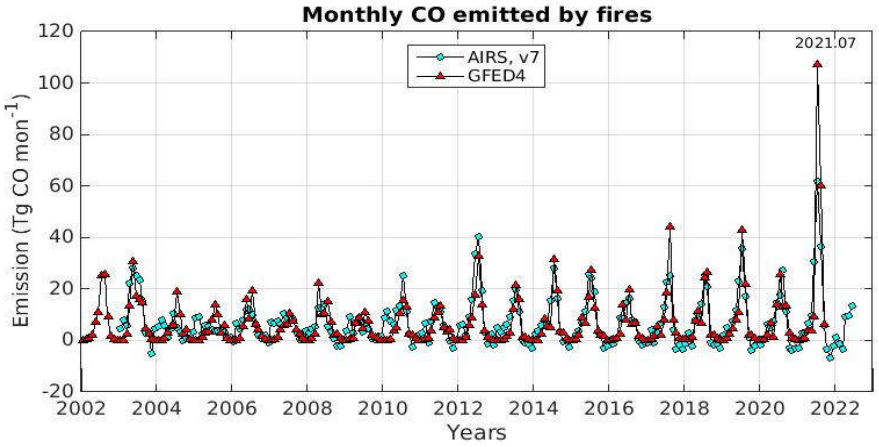

Figure 3. Monthly CO emissions from fires estimated from AIRS data and compared with GFED4 results [3].

Annual CO emissions from AIRS and GFED4 are shown in Figure 5 and Table 2. Corresponding CO_2 emissions (for GFED4 only) are plotted in Figure 5 for comparison. After two years of severe fires in 2002 and 2003 [9] a relatively gradual increase in annual emissions was observed. Regression lines over 2004-2020 for AIRS (red) and for GFED4 (blue) are almost parallel: the slopes are 3.6 ± 2.2 and 3.5 ± 1.3 Tg CO year^{-2}, respectively. Fire emission of CO_2 increases at a rate 43.6 ± 17 Tg CO_2 yr^{-2}. Relative trends are: 4.8 ± 2.7, 5.1 ± 1.9, and 4.8 ± 1.9 % yr^{-1} for AIRS CO, GFED4 CO, and GFED4 CO2, respectively. 95% confidence intervals were obtained as described in [20]. The 2021 fires set a new record with AIRS detected 89% more CO emissions compared to the 2004-2020 average, and GFED4 detecting 182% more.

Preprints (www.preprints.org) | NOT PEER-REVIEWED | Posted: 19 August 2022 doi:10.20944/preprints202208.0360.v1

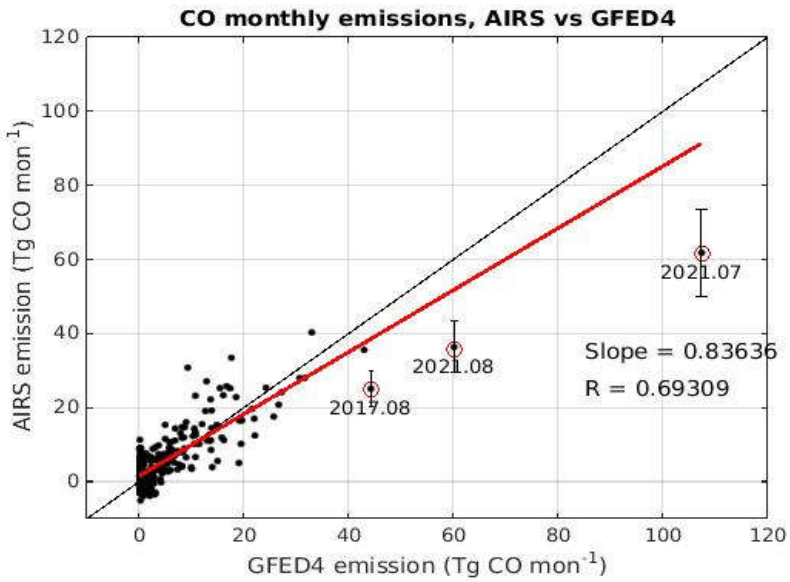

Figure 4. Monthly CO emitted by fires in HNH according to AIRS in comparison with GFED4 data [3]. Times for most scattered points are labeled. Error bars ± 19% here and in Figure 5 correspond to accuracy of correction for reduced sensitivity.

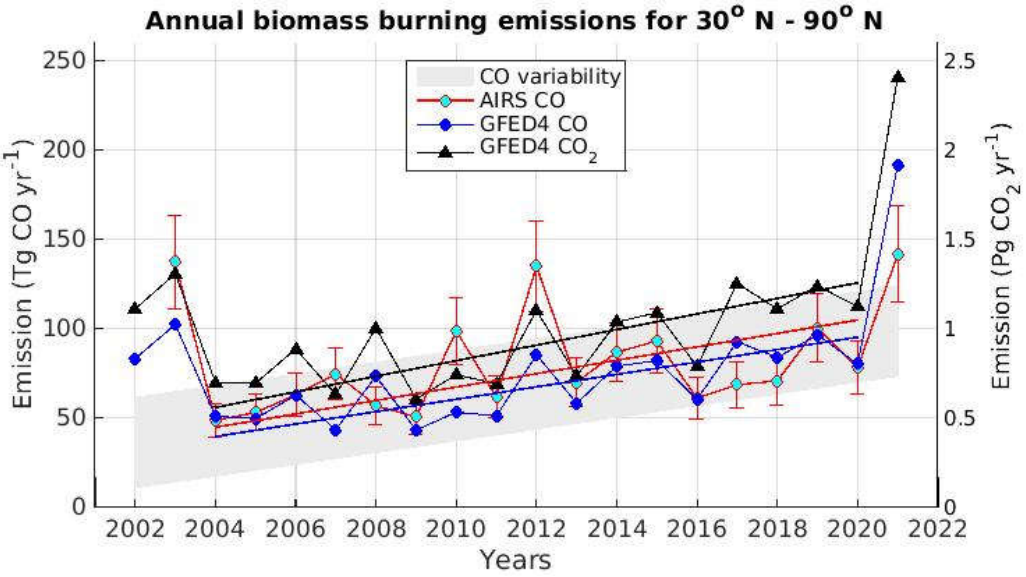

Figure 5. Annual CO emitted by fires in HNH according to AIRS data and a bottom-up GFED4 estimates [3]. CO_2 emission (right scale) is plotted for comparison [3]. Least squares regression lines are shown as well. Error bars follow from validation and estimated as ± 19%. Shaded area corresponds to GFED4 CO ± 2 STD (standard deviation) of the yearly points.

Preprints (www.preprints.org) | NOT PEER-REVIEWED | Posted: 19 August 2022 doi:10.20944/preprints202208.0360.v1

Table 2. Annual HNH CO fire emissions in Tg yr^{-1} for this paper and from [9]. FTIR stands for Furrier Transform Infrared ground-based spectrometers.

Year	AIRS (this paper)	GFED4 (this paper)	FTIR [9]	MOPITT [9]
1998		114	151.4	
1999		48	32.3	
2000		50	-1.8	1.8
2001		43	5.1	-0.9
2002		83	120.6	118
2003	125	103		
2004	49	51		
2005	53	50		
2006	63	63		
2007	75	44		
2008	57	74		
2009	51	43		
2010	99	53		
2011	62	51		
2012	135	85		
2013	70	58		
2014	87	79		
2015	93	82		
2016	61	61		
2017	69	93		
2018	71	84		
2019	101	97		
2020	78	80		
2021	142	192		

4. Discussion and Conclusions

Top-down MOPITT analysis of global and regional CO balance up to 2017 [11] and specifically for wildfires in 2000-2019 [12] did not allow making an unambiguous conclusion about the long-term trend of CO emissions from biomass combustion. For example, the absence of a statistically significant trend in the global CO wildfire emission contradicts a certain decrease in burned areas. Meanwhile, according to [12, p. 2], " Canada and Alaska is the region where both burned areas and emission intensities increased rapidly, driving a substantial increase in its fire CO_2 emissions from the 2000s to the 2010s.". The inverse global modeling used in these two studies is very complex. We believe that our simple box model based on AIRS data without the initial prior requirement and applied to HNH may help clarify of this practical and scientifically important issue.

The point of accuracy is important. A box model inversion of the July 2021 AIRS data (Figures 3 and 4) provided only half of the GFED4 estimate. The 2021 annualized GFED4 CO was also significantly higher AIRS one. This discrepancy does not look as a random fluctuation. We consider this underestimation to be the result of unaccounted for effect of reduced sensitivity of AIRS CO to lower altitudes in the case of the strongest fire season. The validation was based on ground truth sites that were far from the burning areas. Thus, an annual emission of 195 Tg CO yr^{-1} should be closer to reality.

Preprints (www.preprints.org) | NOT PEER-REVIEWED | Posted: 19 August 2022 doi:10.20944/preprints202208.0360.v1

According to estimates based on box model analysis (Figure 5 and Table 2) total CO emissions from biomass burning in the HNH was mostly in the range 50-100 Tg CO yr^{-1}. For three years (2003, 2012, and 2021) wildfires emitted 125, 135 , and 142 Tg CO yr^{-1}, respectively. A similar pattern of year-to-year CO emissions follows from the GFED4 data base, except 2012. After excluding the marginal values for 2003 and 2021, both approaches show a statistically significant positive trend of 4.8-5.1 % yr^{-1}. The record high top-down and bottom-up emission estimates for 2021 support the finding of on increase in HNH biomass burning (mostly boreal fires) over the past decade. The possibility of further acceleration can not be ruled out.

A 20-year data set (Fig. 5) allows us to propose a classification of fires depending on their intensity. All years with emissions within the shaded area can be considered as years with *normal* fires. The fires of 2002, 2003 and 2021 can be classified as *catastrophic* (or *megafires*). Megafires happen from time to time and are likely due to long-lasting blockages in high pressure systems (heat waves) and severe droughts. Such a classification can contribute to more reliable forecasting of various types of forest fires.

Remote sensing satellite measurements combined with a box model allow rapid, almost immediate tracking of CO emissions from forest fires on a hemispheric or global scale. Despite several necessary simplifications, comparison with the GFED4 bottom-up approach improves the validity of our findings. A further improvement of this technique could be a combination with CTM, for example to quantify CO transport and photochemical sink. This model is not an alternative to comprehensive inverse modeling, but is a means of additional verification of the final conclusions. This study focuses on the HNH as an important populated and industrialized area; forest fires can be a serious threat to it.

Author Contributions: Conceptualization, writing, validation, formal analysis, L.Y. Validation and data curation, V.R. .Both authors have read and agreed to the published version of the manuscript.

Funding: The study was funded in part by the Ministry of Science and Higher Education of the Russian Federation under agreement # 075-15-2020-776.

Data Availability Statement: AIRS datasets: AIRS3STM_7.0, AIRS3STD_7.0 https://disc.gsfc.nasa.gov/datasets/; GFED4: https://www.geo.vu.nl/~gwerf/GFED/GFED4/; TCCON: https://data.caltech.edu/records/20140.

Acknowledgments: The authors express gratitude to Andrey Lapenis (University of Albany, New York, USA) for helpful discussions, to Guido van der Werf (Vrije Universiteit Amsterdam, the Netherlands) for detail explanation of GFED4 data set, and to Debra Wunch (University of Toronto, Ontario, Canada) for a guidance in using TCCON validation data.

Conflicts of Interest: The authors declares no conflict of interest.

Preprints (www.preprints.org) | NOT PEER-REVIEWED | Posted: 19 August 2022 doi:10.20944/preprints202208.0360.v1

Appendix

Table A1. Monthly mean characteristic times for air exchange between high and low northern Hemispheres τ_{trans} and photochemical life-time τ_{chem}.

Month	τ_{trans} (months)	τ_{chem} (months)
1	1.7	23.8
2	2.1	14.0
3	3.5	6.5
4	3.4	3.4
5	2.1	2.1
6	1.5	1.4
7	1.5	1.4
8	1.6	1.8
9	2.4	3.5
10	2.6	7.3
11	2.8	15.8
12	1.5	27.2

Table A2 Trend, fifth order polynomial determined for Februaries-Marches for all years and extrapolated onto the rest of data, Xco (ppb).

Month/Year	2003	2004	2005	2006	2007	2008	2009	2010	2011	2012
1	10.4	10	9.1	7.7	6.2	4.7	3.3	2.1	1	0.1
2	10.4	10	9	7.6	6.1	4.6	3.2	2	0.9	0
3	10.4	9.9	8.9	7.5	5.9	4.4	3.1	1.9	0.8	-0.1
4	10.4	9.9	8.8	7.3	5.8	4.3	3	1.8	0.8	-0.1
5	10.3	9.8	8.6	7.2	5.7	4.2	2.9	1.7	0.7	-0.2
6	10.3	9.7	8.5	7.1	5.6	4.1	2.8	1.6	0.6	-0.3
7	10.3	9.6	8.4	7	5.4	4	2.7	1.5	0.5	-0.3
8	10.2	9.5	8.3	6.8	5.3	3.9	2.6	1.4	0.5	-0.4
9	10.2	9.4	8.2	6.7	5.2	3.8	2.5	1.4	0.4	-0.5
10	10.2	9.3	8.1	6.6	5.1	3.6	2.4	1.3	0.3	-0.5
11	10.1	9.2	7.9	6.4	4.9	3.5	2.3	1.2	0.2	-0.6
12	10.1	9.2	7.8	6.3	4.8	3.4	2.2	1.1	0.2	-0.7

Month/Year	2013	2014	2015	2016	2017	2018	2019	2020	2021
1	-0.8	-1.6	-2.4	-3.3	-4.2	-5.3	-6.4	-7.5	-8.3
2	-0.8	-1.6	-2.4	-3.3	-4.3	-5.4	-6.5	-7.6	-8.4
3	-0.9	-1.7	-2.5	-3.4	-4.4	-5.5	-6.6	-7.6	-8.4
4	-1	-1.8	-2.6	-3.5	-4.5	-5.6	-6.7	-7.7	-8.5
5	-1	-1.8	-2.7	-3.6	-4.6	-5.7	-6.8	-7.8	-8.5
6	-1.1	-1.9	-2.7	-3.7	-4.7	-5.8	-6.9	-7.8	-8.5
7	-1.2	-2	-2.8	-3.7	-4.8	-5.9	-6.9	-7.9	-8.6
8	-1.2	-2	-2.9	-3.8	-4.9	-5.9	-7	-8	-8.6
9	-1.3	-2.1	-3	-3.9	-4.9	-6	-7.1	-8	-8.6
10	-1.4	-2.2	-3	-4	-5	-6.1	-7.2	-8.1	-8.7
11	-1.4	-2.2	-3.1	-4.1	-5.1	-6.2	-7.3	-8.2	-8.7
12	-1.5	-2.3	-3.2	-4.2	-5.2	-6.3	-7.4	-8.3	-8.7

Preprints (www.preprints.org) | NOT PEER-REVIEWED | Posted: 19 August 2022 doi:10.20944/preprints202208.0360.v1

Table A3 Seasonal cycle of Xco in HNH, calculated for period 2004.01 - 2007.12.

Month	Seasonal cycle, ppb
1	8.0
2	13.5
3	17.5
4	17.7
5	7.1
6	-6.8
7	-12.6
8	-13.3
9	-14.0
10	-11.9
11	-6.1
12	0.9

References

1 Kasischke, E; Stocks, B. *Fire, climate change, and carbon cycling in the boreal forest*; Springer-Verlag: New York, NY, USA, 2000; 461 p.

2 Seiler, W.; Crutzen, P.J. Estimates of gross and net fluxes of carbon between the biosphere and the atmosphere from biomass burning. *Clim. Change* **1980,** *2,* 207–247

3 Van der Werf, G. R.; Randerson, J. T.; Giglio, L.; van Leeuwen, T. T.; Chen, Y.; Rogers, B. M.; Mu, M; van Marle, M. J. E.; Morton, D. C.; et al. Global fire emissions estimates during 1997–2016. *Earth Syst. Sci. Data* **2017,** 9, 697–720 .

4 Giglio, L.; Csiszar, I.; Justice, C. O. Global distribution and seasonality of active fires as observed with the Terra and Aqua Moderate Resolution Imaging Spectroradiometer (MODIS) sensors. J. *Geophys. Res.-Biogeo*. **2006,** *111*, G02016, https://doi.org/10.1029/2005JG000142,.

5 Dekker, I. N.; Houweling, S.; Aben, I.; Röckmann, T.; Krol, M.; Martínez-Alonso, S.; Deeter, M. N.; Worden, H. M. Quantification of CO emissions from the city of Madrid using MOPITT satellite retrievals and WRF simulations. *Atmos. Chem. Phys*. **2017,** *17*, 14675–14694

6 Bela, M. M.; Kille, N.; McKeen, S. A.; Romero-Alvarez, J.; Ahmadov, R.; James,E.; Pereira, G.; Schmidt, C.; Pierce, R. B.; O'Neill, S. M., et al. Quantifying carbon monoxide emissions on the scale of large wildfires. *Geophys. Res. Lett.* **2021**, 49(3):e2021GL095831. https://doi.org/10.1029/2021GL095831

7 Deeter, M.; Francis, G.; Gille, J.; Mao, D.; Martínez-Alonso, S.; Worden, H.; McKain, K. The MOPITT Version 9 CO product: Sampling enhancements and validation. *Atmosph. Meas. Tech.*, **2022** *15*, 2325-2344. doi:10.5194/amt-15-2325-2022

8 Aumann, H. H. ; Chahine, M. T.; Gautier, C.; Goldberg M. D.; Kalnay,E.; McMillin, L. M.; Revercomb, H.P.; Rosenkranz, P.W.; Smith, W. L.; Staelin, D. H. et al. AIRS/AMSU/HSB on the Aqua mission: design, science objectives, data products and processing systems. *IEEE Trans. Geosci. Rem. Sens*. **2003,** *41*, 253-264.

9 Yurganov, L. N.; Duchatelet, P.; Dzhola, A. V.; Edwards, D. P.;Hase, F.; Kramer, I.; Mahieu, E.; Mellqvist, J.; Notholt, J.; Novelli, P. C.; Rockmann, et al. .: Increased Northern Hemispheric carbon monoxide burden in the troposphere in 2002 and 2003 detected from the ground and from space. *Atmos. Chem.Phys*., **2005,** *5*, 563–573, doi:10.5194/acp-5-563-2005,.

10 Yurganov, L. N.; Blumenstock, T.; Grechko, E. I.; Hase, F.; Hyer,E. J.; Kasischke, E. S.; Koike, M.; Kondo, Y.; Kramer, I.; Le-ung, F.-Y., et al. A quantitative assessment of the 1998 carbon monoxide emission anomaly in the northern Hemisphere based on total column and surface concentration measurements. *J. Geophys. Res.*, **2004.** *109*, D15305, doi:10.1029/2004JD004559,.

11 Zheng, B.; Chevallier, F.; Yin, Y.; Ciais, P.; Fortems-Cheiney, A.; Deeter, M. N.;R. J. Parker,Y. Wang, H. M. Worden, Zhao, Y. . Global atmospheric carbon monoxide budget 2000-2017 inferred from multi-species atmospheric inversions. *Earth Syst. Sci. Data* **2019,** *11*, 1411-1436. doi:10.5194/essd-11-1411-2019

12 Zheng, B.; Ciais, P. ; Chevallier A. ; Chuvieco, E.; Chen, Y. ; Yang. H. Increasing forest fire emissions despite the decline in global burned area. *Sci. Adv*. **2021,** 7 : eabh2646

13 Tian, B.; Manning, R. J.; Thrastarson, H.; Fetzer, E.; Monarrez, R. AIRS Version 7 Level 3 product user guide. **2020** https://docserver.gesdisc.eosdis.nasa.gov/public/project/AIRS/V7_L3_User_Guide.pdf.

14 Wunch, D.; Toon, G. C.; Blavier, J.-F. L.; Washenfelder, R. A.; Notholt, J.; Connor, B. J.; Griffith, D. W. T.; Sherlock, V.; Wennberg, P. O. The Total Carbon Column Observing Network. *Philosophical Transactions of the Royal Society A: Mathematical, Physical and Engineering Sciences* **2011,** *369*, 2087-2112,.

15 Rakitin, V.S.; Elansky, N.F.; Skorokhod, A.I. ; Dzhola, A. V. ; Rakitina, A. V. ; Shilkin, A. V. ; Kirillova, N. S.; Kazakov A. V.. Long-Term Tendencies of Carbon Monoxide in the Atmosphere of the Moscow Megapolis. *Izv. Atmos. Ocean. Phys.* **2021**, *57*, 116–125 https://doi.org/10.1134/S0001433821010102

16 Holloway, T.; Levy II,H.; Kasibhatla,P. Global distribution of carbon monoxide. *J. Geophys. Res.*, **2000**, *105*, 12,123 – 12,147,.

Preprints (www.preprints.org) | NOT PEER-REVIEWED | Posted: 19 August 2022 doi:10.20944/preprints202208.0360.v1

17 Spivakovsky, C. M.; Logan, J. A.; Montzka, S. A.; Balkanski, Y. J.; Foreman-Fowler, M.; Jones, D. B. A.; Horowitz, L. W.; Fusco, A. C.; Brenninkmeijer, C. A. M.; Prather, M. J.; et al. Three-dimensional climatological distribution of tropospheric OH: Update and evaluation. *J. Geophys. Res.* **2000,** *105(D7)*, 8931–8980.

18 DeMore, W. B.; Sander, S. P.; Golden, D. M.; Hampson, R. F.;Kurylo, M. J.; Howard, C. J.; Ravishankara, A. R.; Kolb, C. E.;and Molina, M. J. Chemical kinetics and photochemical data for use in stratospheric modeling. *JPL Publ.*,**1997**, *97*-4,.

19 Dianov-Klokov, V. I. ; Yurganov, L. N. A spectroscopic study of the global space-time distribution of atmospheric CO. *Tellus* **1981,** *33*, 262–273.

20 Chatterjee, S.; Hadi, A. S. Influential observations, high leverage points, and outliers in linear regression. *Stat. Sci*. **1986,** *1*, . 379-416.